Giant magnetoresistance in Co-Fe-Cu granular ribbons

2000 J. Phys.: Condens. Matter 12 4829

(http://iopscience.iop.org/0953-8984/12/22/315)

J. Phys.: Condens. Matter **12** (2000) 4829–4835. Printed in the UK PII: S0953-8984(00)11288-3

Giant magnetoresistance in Co–Fe–Cu granular ribbons

F Wang, Z D Zhang†, T Zhao, M G Wang, D K Xiong, X M Jin, D Y Geng, X G Zhao, W Liu and M H Yu

International Centre for Materials Physics, Institute of Metal Research, Academia Sinica, Shenyang 110015, People's Republic of China

E-mail: zdzhang@imr.ac.cn

Received 24 January 2000, in final form 4 April 2000

Abstract. The structure and magnetoresistance of as-quenched and annealed $Co_{15-x}Fe_xCu_{85}$ ($x = 0, 3, 6, 9, 12, 15$) granular alloys have been investigated. Co–Fe–Cu nanoparticles with sizes in the range of 2–3 nm, 10–20 nm and ∼100 nm are embedded in a Cu matrix in Co–Fe–Cu granular ribbons. The giant magnetoresistance of the granular alloys decreases with increasing Fe content. The Co–Fe–Cu nanoparticles with large size result in a decrease of the number of nanoparticles, the interfaces for spin-dependent scattering of electrons and thus the magnetoresistance.

1. Introduction

Since the discovery of giant magnetoresistance (GMR) in granular solids [1, 2], the electrical resistivity of heterogeneous granular Co–Cu [3], Co–Ni–Fe [4, 5], Co–Ag [6], Fe–Ag [7], Fe–Ni–Ag [8], Ni–Co–Ag [9], Co–Cu [10], Fe–Ni–Cu [11] and Fe–Co–Cu [12] thin films have been studied. It has been well known that the size distribution of the magnetic nanoparticles plays an important role in this phenomenon. It is widely accepted [3, 13] that the phase segregation in Co–Cu granular ribbons is a nucleation and growth process. It was reported that the phase segregation of Co–Ni–Fe [4, 5], Co–Ni–Cu [13] ribbons is spinodal decomposition. It also has been found that the MR ratio decreases in the Co–Ni–Cu and Co–Ni–Fe granular ribbons, when these materials are cooled from room temperature to low temperature.

In our previous paper [14], the GMR and the microstructure in $Co_{20}Ni_xCu_{80-x}$ ($x = 5$, 10, 15 and 20) granular ribbons prepared by melt spinning were reported. It was found that the phase segregation in the Co–Ni–Cu ribbons is not a pure nucleation decomposition or growth process. It is closely connected with the Ni content. In particular, in the Co–Ni–Cu granular ribbons with low Ni content, the magnetoresistance ratio is larger than in Co–Cu granular ribbons. In contrast to the ribbons with high Ni content [13], the low-Ni-content ribbons show an increase in magnetoresistance $\Delta R/R$ at low temperatures.

In the present work, we study the structure and magnetoresistance of as-quenched and annealed $Co_{15-x}Fe_xCu_{85}$ ($x = 0, 3, 6, 9, 12, 15$) granular alloys.

2. Experimental details

$Co_{15-x}Fe_xCu_{85}$ ribbons with $x = 0, 3, 6, 9, 12$ and 15 were prepared by melt spinning on a copper wheel in Ar atmosphere at wheel speeds of about 35 or 41 m s^{-1}. In order to maximize

† Correspondence to: Zhang Zhi-dong.

0953-8984/00/224829+07$30.00

the magnetoresistance, the prepared ribbons of about 2 mm wide and 20 to 30 μm thick were annealed in the temperature range from 520 to 970 K. The electrical resistivity was measured by the standard dc four-terminal method. The magnetization was measured in the temperature range from 5 to 300 K and in magnetic fields up to 5 T, by using a superconducting quantum interference device (SQUID) magnetometer. The crystal structure was characterized by x-ray diffraction (XRD). The averaged chemical composition and the homogeneity of the ribbons were checked by means of a JSM-6301F scanning electron microscope (SEM) and an electron microprobe (EM). The microstructures of the ribbons were also studied by using a Philips FM420 analytic electron microscope (AEM) operated at 100 kV.

3. Results and discussion

Figure 1 shows XRD patterns of as-quenched $Co_{15-x}Fe_xCu_{85}$ ($x = 0$, 3 and 15) granular ribbons in the low-angle region. The peaks in the XRD pattern of as-quenched Co–Cu ribbons can be indexed to belong to the Co-rich and Cu-rich phases (the lowest curve in figure 1). As Fe is added, the peaks of the Co-rich phase are not observable in the as-quenched $Cu_{12}Fe_3Cu_{85}$ ribbons (the middle curve in figure 1). Upon introduction of Fe, the position of the peak of the Cu-rich phase moves slightly towards lower angle, because the atomic size of Fe is larger than that of Co. The (110) diffraction peak of α-Fe appears when Co is completely substituted by Fe (the uppermost curve in figure 1).

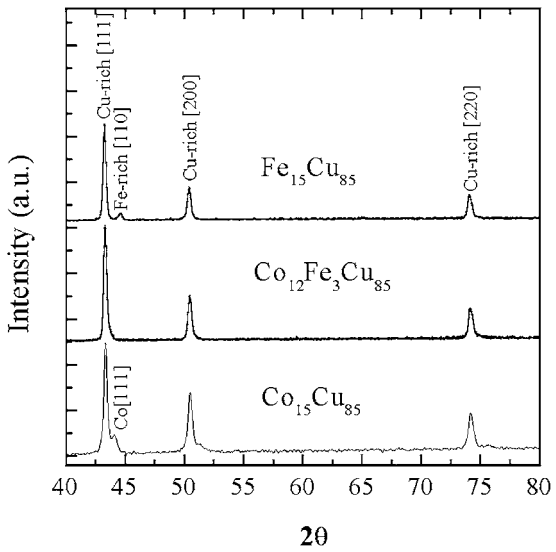

Figure 1. X-ray-diffraction patterns of as-quenched $Co_{15-x}Fe_xCu_{85}$ ($x = 0$, 3 and 15) ribbons.

The ribbons are polycrystalline with a grain size of hundreds of nanometres, as determined by means of AEM and XRD. Figure 2 shows the analytic electron microscope micrographs of as-quenched $Co_6Fe_9Cu_{85}$ ribbons. The microstructure of $Co_6Fe_9Cu_{85}$ ribbons is similar to that in the Co–Cu ribbons [15]. Namely, magnetic particles are embedded in the polycrystalline Cu matrix. However, the size of the particles in the Co–Fe–Cu ribbons is much larger than that of the Co–Cu ribbons. The composition of the particles in the Co–Fe–Cu ribbons is complex. The amount of particles of rich FeCo phases increases with increasing Fe content. Table 1 lists the composition of two kinds of particle (with sizes of 10–20 nm and 100 nm, respectively),

measured by means of energy spectrum analysis of AEM. The size and the distribution of the two kinds of magnetic nanoparticle may play an important role in magnetic and transport properties.

Figure 2. Analytic electron microscope micrographs of as-quenched $Co_6Fe_9Cu_{85}$ ribbons.

Table 1. Results of energy spectra analysis of AEM for as-quenched $Co_6Fe_9Cu_{85}$ ribbons. Small particles and large particles are in the range of 10–20 nm and 100 nm, respectively.

Composition	Small particles	Large particles	Matrix
Co (at.%)	11.5	23.4	4.9
Fe (at.%)	13.8	33.9	5.9
Cu (at.%)	74.7	42.7	89.2

Figure 3 represents x-ray diffraction patterns of $Co_{12}Fe_3Cu_{85}$ ribbons annealed at 620 K, 750 K and 870 K for 10 min, respectively. After annealing at 870 K for 10 min, the peaks corresponding to Co-rich and CoFe-rich phases appear in the XRD pattern of the sample with 3 at.% Fe. Meanwhile, the diffraction peaks of Cu shift toward the lower angles when the Fe content is increased. This is due to the separation of Co, Fe atoms from the Cu matrix, which leads to the shift of the peaks of rich-Cu matrix toward those of pure Cu. Correspondingly the lattice parameter is enhanced with increasing Fe content.

The resistivity of the Co–Fe–Cu ribbons is determined to be varied in the range of 10–60 $\mu\Omega$ cm, depending on the composition, the conditions of preparation (such as, wheel speed, annealing temperature and annealing time) and also the applied magnetic field. The substitution of Fe for Co strongly affects the magnetoresistance of Co–Cu ribbons. The magnetoresistance of as-quenched Co–Fe–Cu ribbons is nearly zero. Even for the ribbons annealed at the optimal annealing temperature of 750 K, the magnetoresistance of the Fe-containing ribbons is much smaller than that of the Co–Cu ribbons. Figure 4 shows the field dependence of the magnetoresistance MR ($= (R_H - R_0)/R_0$) ratio at room temperature for the samples with various Fe contents after annealing at 750 K for 10 min. The MR ratio decreases with increasing Fe content. The MR ratio at room temperature of $Co_{12}Fe_3Cu_{85}$ and $Co_9Fe_6Cu_{85}$ are 1.7 and 0.6% in 1.2 T, respectively, which are much lower than those of $Co_{15}Cu_{85}$ (4.6%) and $Co_{20}Ni_5Cu_{75}$ (6.2%) [14]. The decrease of the MR ratio upon

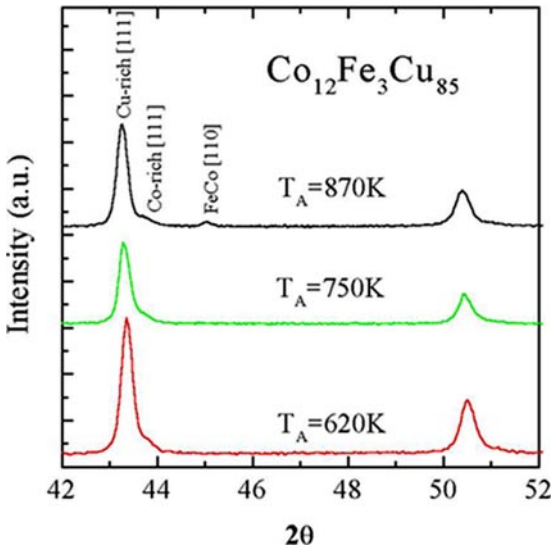

Figure 3. X-ray diffraction patterns of $Co_{12}Fe_3Cu_{85}$ ribbons annealed at 620 K, 750 K and 870 K for 10 min.

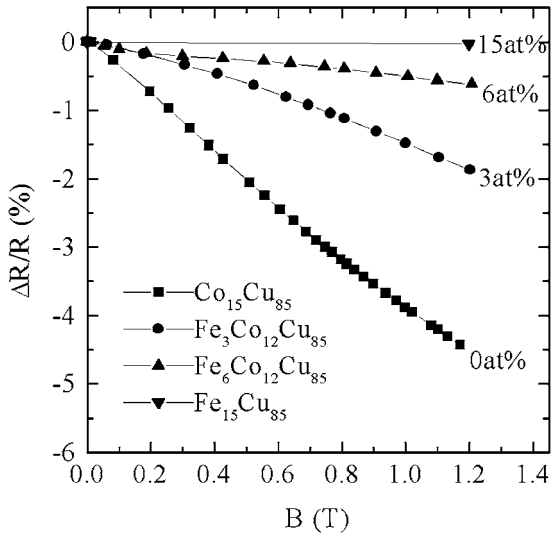

Figure 4. Field dependence of the magnetoresistance at room temperature for $Co_{15-x}Fe_xCu_{85}$ ($x = 0, 3, 6, 15$) after annealing at 750 K for 10 min.

Fe substitution is in good agreement with the results in Co–Fe–Cu sputtered samples [16]. However, this effect is more evident in the present system. An explanation of this result may be that the number of magnetic CoFe–rich particles with small size (2–3 nm) increases in the Co–Fe–Cu granular ribbons, comparable to what happens in the Co–Cu granular ribbons. Meanwhile, the magnetic particles with large size (100 nm) appear. Therefore, the number of interfaces decreases, which is of benefit to the spin-dependent scattering of electrons.

The magnetoresistance at room temperature of melt-spun $Co_{15}Cu_{85}$ and $Co_{12}Fe_3Cu_{85}$ ribbons with different wheel speeds after annealing at 750 K for 10 min is given in figure 5. The MR ratio of the ribbons decreases with increasing wheel speeds. This is in contradiction with the expectation that the high rate of cooling decreases the size of Co-rich separation in the Cu matrix, and thus enhances the magnetoresistance effect. Although this effect still exists, there might be other factors that are dominant in the present system. First, the large amount of superparamagnetic particles in the Cu matrix increase the saturation field rapidly. This results in the low values of the MR ratio at the applied field of 1.2 T that is much lower than the saturation field. Second, the decrease of the particles' size results in the increase of grain boundaries, and correspondingly the increase of defects. This raises the resistivity ρ, and reduces the relative variation of the resistivity $\Delta\rho/\rho$. It is understood that in the polycrystalline ribbons, several mechanisms for the spin-dependent scattering compete with each other and that the magnetoresistance depends on which mechanism is dominant.

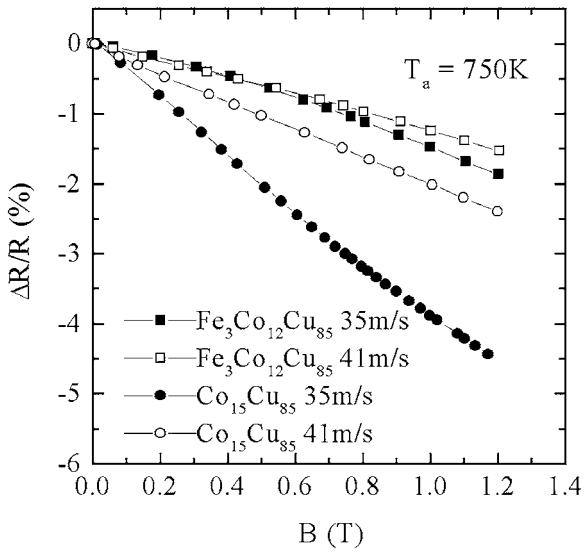

Figure 5. Magnetoresistance at room temperature of melt-spun $Co_{15}Cu_{85}$ and $Co_{12}Fe_3Cu_{85}$ ribbons with different wheel speeds after annealing at 750 K for 10 min.

The MR ratio of $Co_{12}Fe_3Cu_{85}$ ribbons depends sensitively on annealing temperature. The results shown in figure 6 indicate that annealing at temperature lower than 620 K does not change the MR ratio evidently. The MR ratio reaches its maximum (1.7%) after annealing at 750 K, and then lowers to 1.5% after annealing at 870 K for 10 min. It is clearly seen from figure 6 that the saturation field of the magnetoresistance is very high for the ribbons annealed at temperatures lower than 750 K. For the ribbons annealed at 870 K, the MR ratio is nearly saturated by an applied field of 1.2 T. This suggests that the separation processes of CoFe-rich, Co-rich phases from the Cu matrix are almost completed at 870 K, which consist of the separation of the phases, the growth of the particles and the disappearance of the defects. This is in consistence with the results of XRD patterns in figure 3.

Figure 7 represents the zero-field-cooled (ZFC) and field-cooled (FC) (in a field of 0.005 T) magnetization curves of an as-quenched $Fe_{15}Cu_{85}$ ribbon. Below a characteristic freezing temperature, a large thermal hysteresis is observed. The thermal hysteresis at temperatures far above the maximum of the ZFC curve suggests the existence of a broad distribution in size

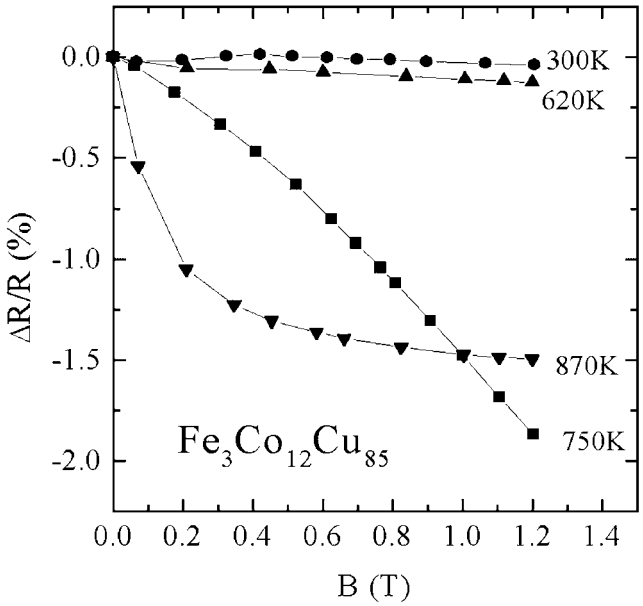

Figure 6. Magnetoresistance at 300 K of $Co_{12}Fe_3Cu_{85}$ granular ribbons after annealing at various temperatures for 10 min.

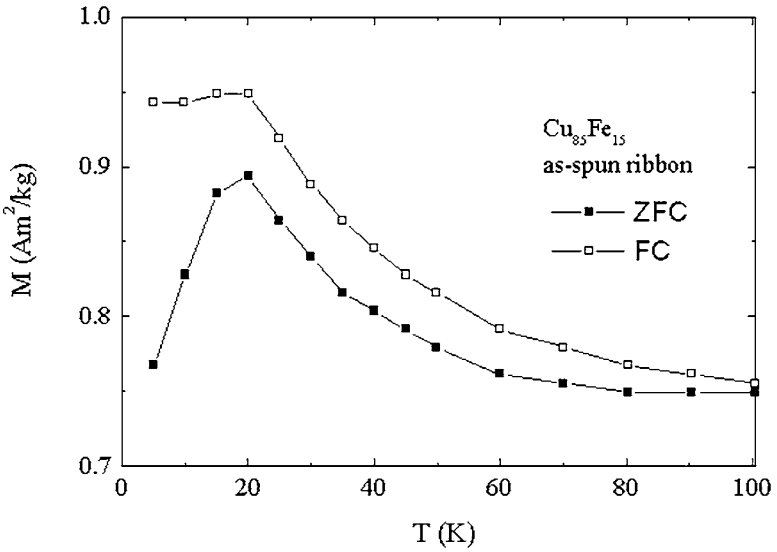

Figure 7. Zero-field-cooled and field-cooled ($B = 0.005$ T) magnetization curves of an as-quenched $Fe_{15}Cu_{85}$ ribbon.

and shape of the magnetic precipitates. The granular ribbon is a disordered magnetic system [3] that should have a rather complex magnetic behaviour. However, the peak in the zero-field-cooled (ZFC) curve of the as-quenched $Fe_{15}Cu_{85}$ ribbon shifts to a lower temperature (about 20 K), compared to that of as-quenched $Co_{20}Ni_5Cu_{75}$ [14] and the Co–Cu ribbons [14, 15].

It is obvious that the magnetoresistance effect in Fe–Cu and Co–Fe–Cu alloys is weaker than that in Co–Cu and Co–Ni–Cu alloys. The main reasons are as follows: (1) The size of the Fe-rich particles is larger than that of Co-rich phases in the grain boundaries and inside the grains. Some Fe-rich particles are even larger than 100 nm, which are out of the condition for spin-dependent scattering. (2) Since the solid solubility of Fe-rich metastable states is larger than that of Co-rich metastable ones, the separation process of Fe-rich magnetic phases is less completed than that of Co-rich phases. Thus the Fe–Cu mixture disordered area of the interfaces of Fe-rich magnetic particles is larger than that of a Co–Cu mixture [17]. This leads to the smaller thickness and diameter of the paramagnetic shells of the interfaces, and correspondingly the smaller effect of the spin-dependent scattering. (3) The mismatch between the lattices of Fe-rich phase (bcc α-Fe phase) and Cu matrix is smaller than that between the lattices of Co-rich phase and Cu matrix. The larger coarseness of boundaries results in the bigger resistivity ρ, and reduces the relative variation of the resistivity $\Delta\rho/\rho$.

4. Summary

In summary, we report the giant magnetoresistance in granular CoFeCu ribbons. Full-grown Co–Fe–Cu nanoparticles are embedded in the Cu matrix in Co–Fe–Cu granular ribbons. The giant magnetoresistance of the granular alloys decreases with increasing Fe content. The large size of Co–Fe–Cu nanoparticles results in the decrease of the numbers of the nanoparticles, the interfaces for spin-dependent scattering of electrons and thus the magnetoresistance.

Acknowledgments

We thank the National Natural Sciences Foundation of China for the support to the projects Nos 59725103, 59831010 and 59871054, the Sciences and Technology Commissions of Shenyang and Liaoning.

References

[1] Berkowitz A E., Mitchell J R, Carey M J, Young A P, Zhang S, Spada F E, Parker F T, Hutten A and Thomas G 1992 *Phys. Rev. Lett.* **68** 3745
[2] Xiao J Q, Jiang J S and Chien C L 1992 *Phys. Rev. Lett.* **68** 3749
[3] Dieny B, Chamberod A, Cowache C, Genin J B, Teixeira S R, Ferre R and Barbara B 1994 *J. Magn. Magn. Mater.* **135** 191
[4] Jin S, Chen L H, Tiefel T H, Eibschutz M and Ramesh R 1994 *J. Appl. Phys.* **75** 6915
[5] Chen L H, Jin S, Tiefel T H and Wu T C 1994 *J. Appl. Phys.* **76** 6814
[6] Xiong P, Xiao G, Wang J Q, Xiao J Q, Jiang J S and Chien C L 1992 *Phys. Rev. Lett.* **69** 3220
[7] Tsoukatos A, Wan H, Hadjipanayis G C, Unruh K M and Li Z G 1993 *J. Appl. Phys.* **73** 5509
[8] Jiang J S, Xiao J Q and Chien C L 1992 *Appl. Phys. Lett.* **61** 2362
[9] Kitada M, Yamamoto K and Shimizu N 1993 *J. Magn. Magn. Mater.* **124** 243
[10] Wecker J, Helmolt R V, Schultz L and Samwer K 1993 *Appl. Phys. Lett.* **62** 1985
[11] Martins C S, Rechenberg H R and Missell F P 1998 *J. Appl. Phys.* **83** 7001
[12] Rubinstein M, Harris V G, Das B N and Koon N C 1994 *Phys. Rev.* B **50** 12 550
[13] Zhang S Y and Cao Q Q 1996 *J. Appl. Phys.* **70** 6261
[14] Wang F, Zhang Z D, Zhao T, Wang M G, Xiong D K, Jin X M, Geng D Y, Zhao X G, Liu W, Yu M H and de Boer F R 2000 *J. Phys.: Condens. Matter* **12** 2525
[15] Wang W D, Zu F W, Weng J, Shao J M and Lai W Y 1997 *J. Chin. Electron. Microsc. Soc.* **16** 290
[16] Wang J Q and Xiao G 1994 *Phys. Rev.* B **49** 3982
[17] Du J H, Li Q, Wang L C, Sang H, Zhang S Y, Du Y W and Feng D 1995 *J. Phys.: Condens. Matter* **7** 9425